GSA Data Repository Item 2019121

Alva-Valdivia, L.M., Agarwal, A., García-Amador, B., Morales-Barrera, W., Agarwal, K.K., Rodríguez, S., and Gonzalez-Rangel, J.A., 2019, Paleomagnetism and tectonics from the late Pliocene to late Pleistocene in the Xalapa monogenetic volcanic field, Veracruz, Mexico: GSA Bulletin, https://doi.org/10.1130/B32006.1.

Data Repository

Figure DR1. χ-T curves demonstrating variation in magnetic susceptibility (A.U. - arbitrary units) with temperature (°C) during heating (black) and cooling (grey) of the samples. The T_Cs during heating are marked by black arrow(s).

Figure DR2. IRM and UnMix curves demonstrating variation in magnetization (A/m) with respect to the applied field (T).

Figure DR3. Representative Hysteresis diagrams revealing the contribution of the coercivity and the saturation of the samples in the applied magnetic field.

Figure DR4. Day plot (after Dunlop, 2002) elucidating the dominant magnetic domain size in the samples by presenting the ratios between Mrs (remanent magnetization) and Ms (saturation remanence), and Hcr (remanence of coercivity) and Hc (coercive force).

Figure DR5. FORC diagrams revealing the contribution of the SD, MD and PSD particles.

Figure DR6. Zijderveld demagnetization plots of three representative specimens with single, double and multiple NRM components.

Table DR1. The measured bulk susceptibility (χ) and the Curie temperatures (Tc1, Tc2, and Tc3) are presented. Site 8 and 16 were not measured.

Table DR2. Rotation (R) and flattening (F) experienced by the Xalapa Basalts, calculated by comparison with the GAPWaP (Torsvik et al., 2012). ΔR and ΔF calculated with the Demarest's method (Demarest, 1983).

Table DR3. Rotation (R) and flattening (F) experienced by the El Castillo Ignimbrite, calculated by comparing ChRM directions provided by Alva-Valdivia et al. (2017) and the GAPWaP (Torsvik et al. 2012). ΔR and ΔF calculated with the Demarest's method (Demarest 1983).

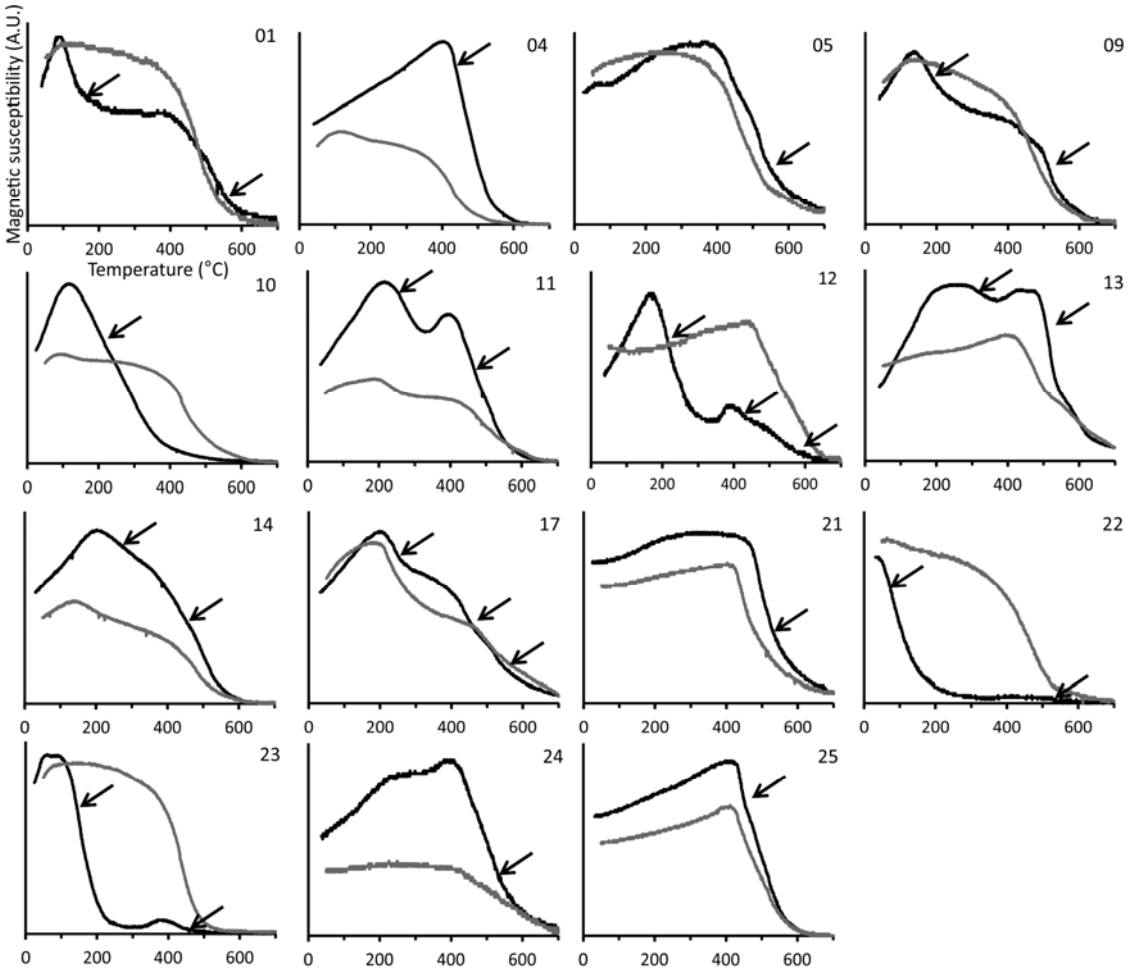

Figure DR1: χ-T curves demonstrating variation in magnetic susceptibility (A.U. - arbitrary units) with temperature (°C) during heating (black) and cooling (grey) of the samples. The T_Cs during heating are marked by black arrow(s).

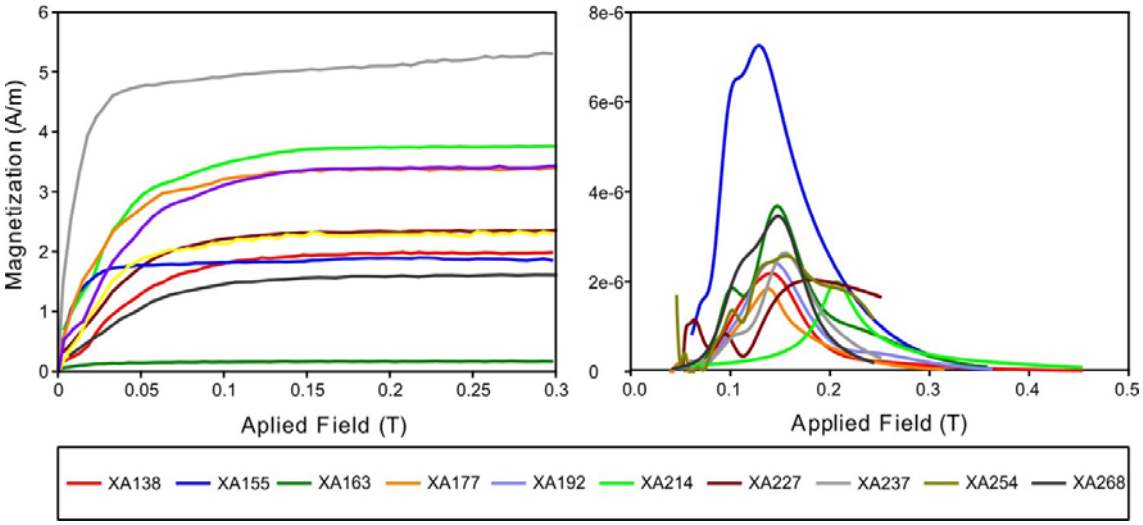

Figure DR2: IRM and UnMix curves demonstrating variation in magnetization (A/m) with respect to the applied field (T).

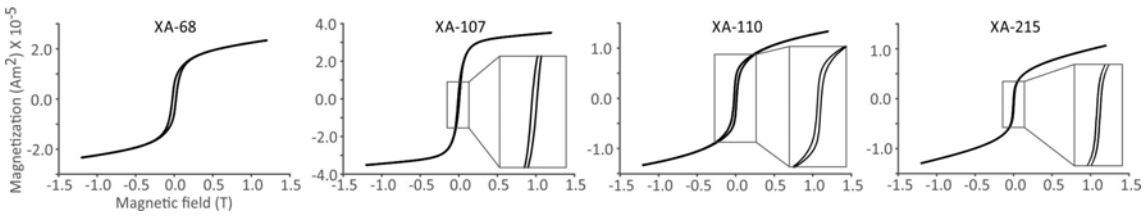

Figure DR3: Representative Hysteresis diagrams revealing the contribution of the coercivity and the saturation of the samples in the applied magnetic field.

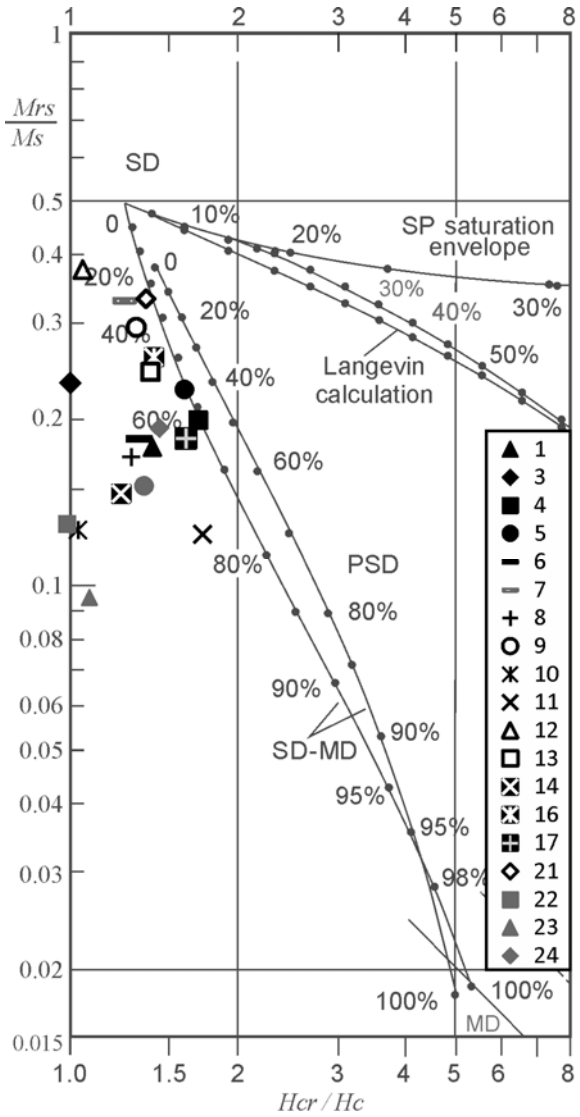

Figure DR4: Day plot (after Dunlop, 2002) elucidating the dominant magnetic domain size in the samples by presenting the ratios between Mrs (remanent magnetization) and Ms (saturation remanence), and Hcr (remanence of coercivity) and Hc (coercive force).

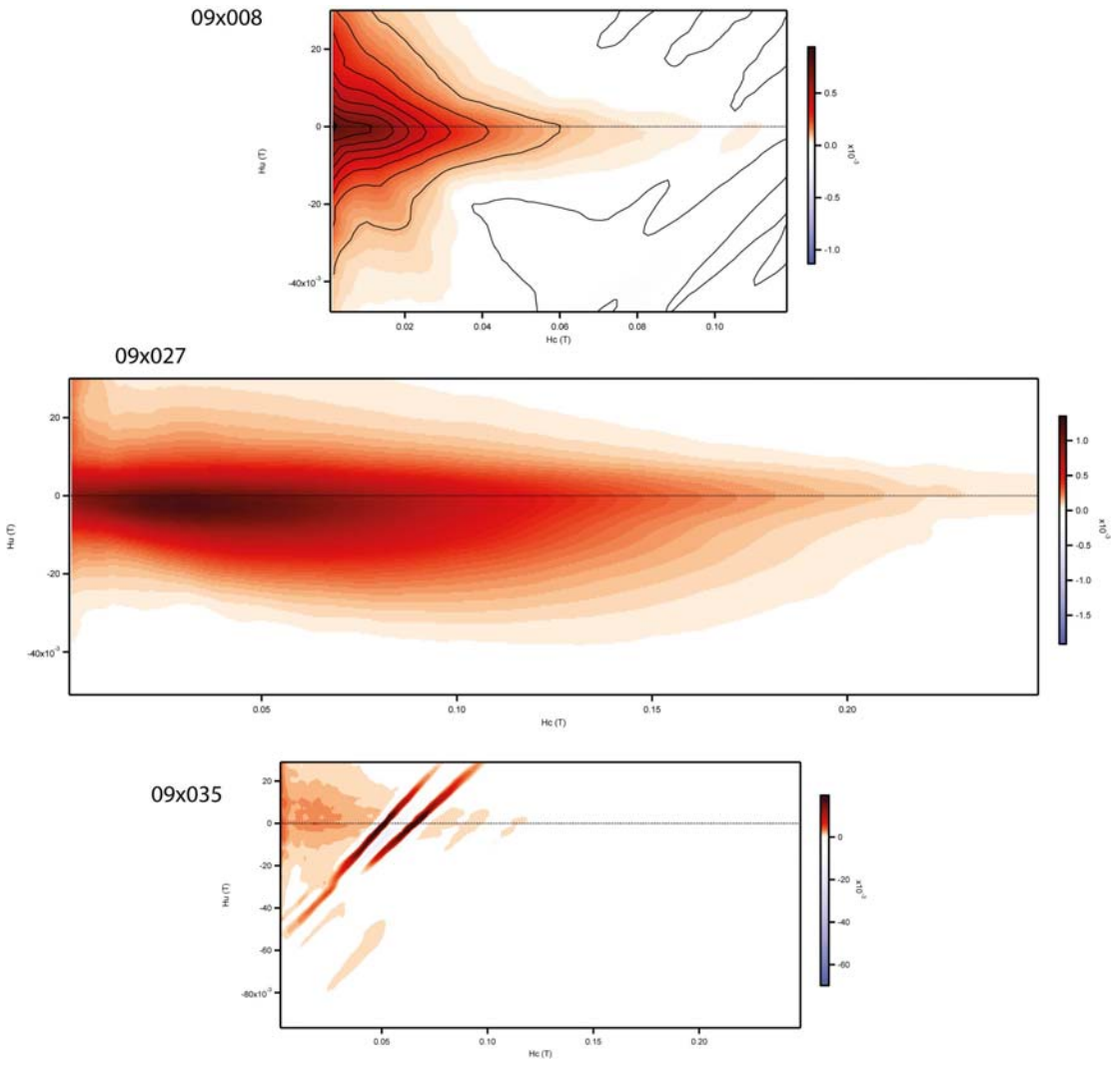
09x008
09x027
09x035
Hu (T)
Hc (T)

09x041

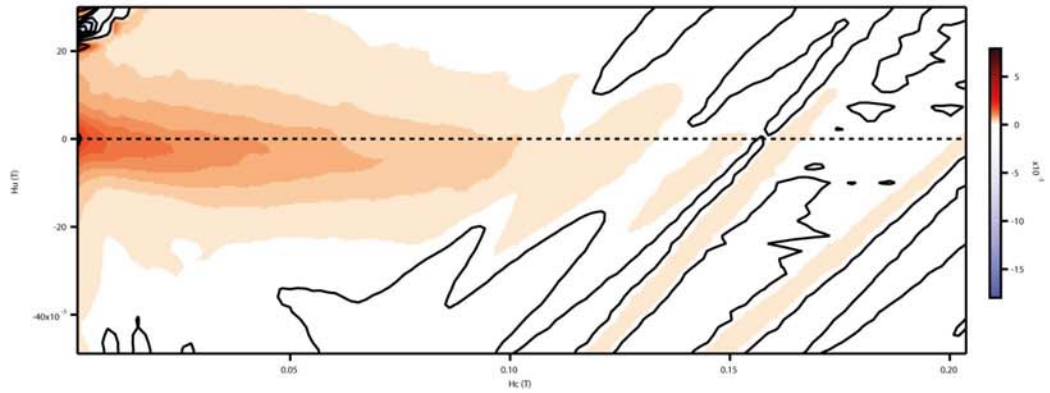

09x061

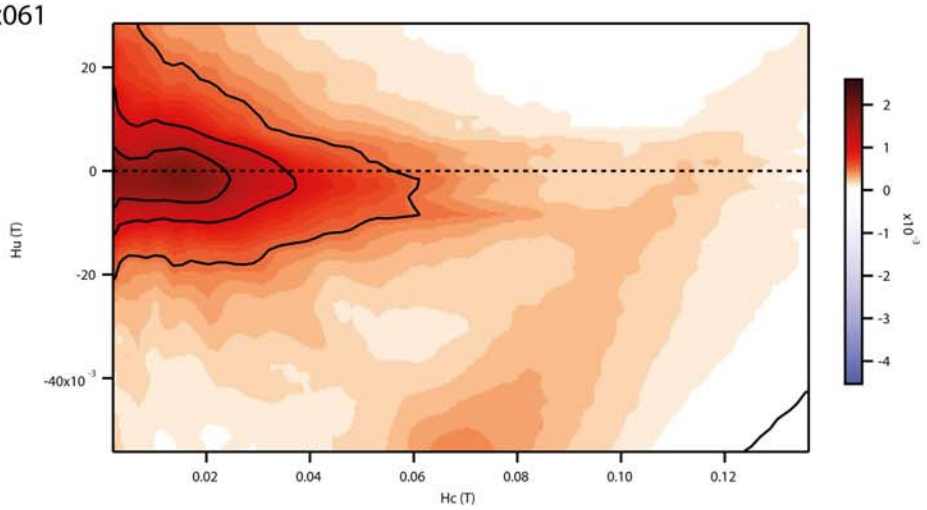

09x076

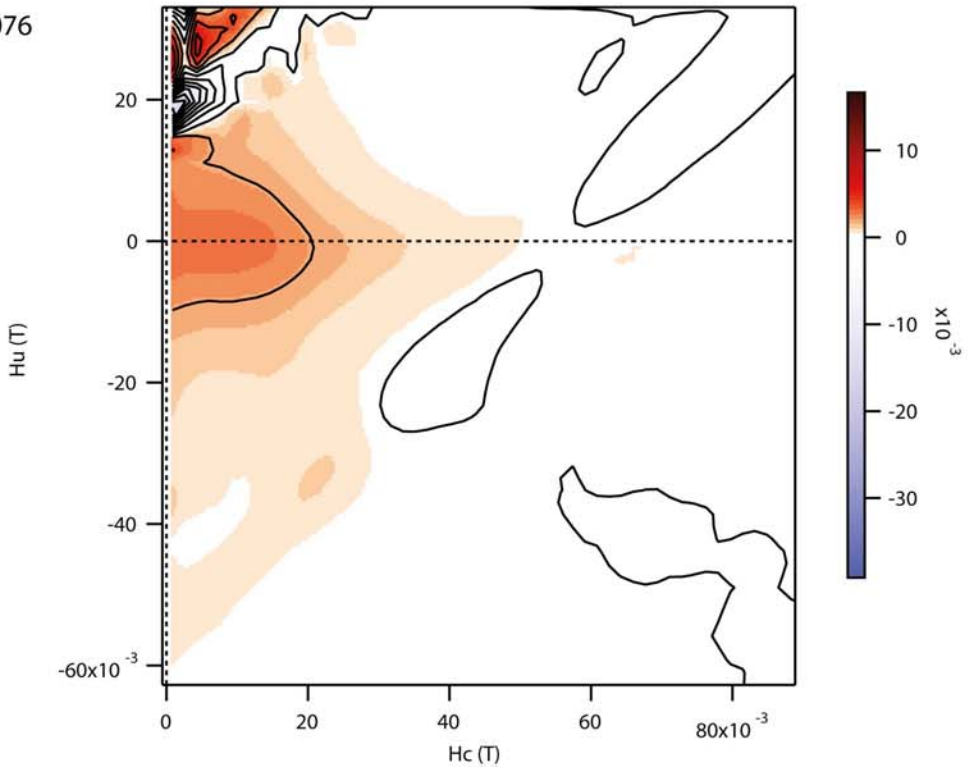

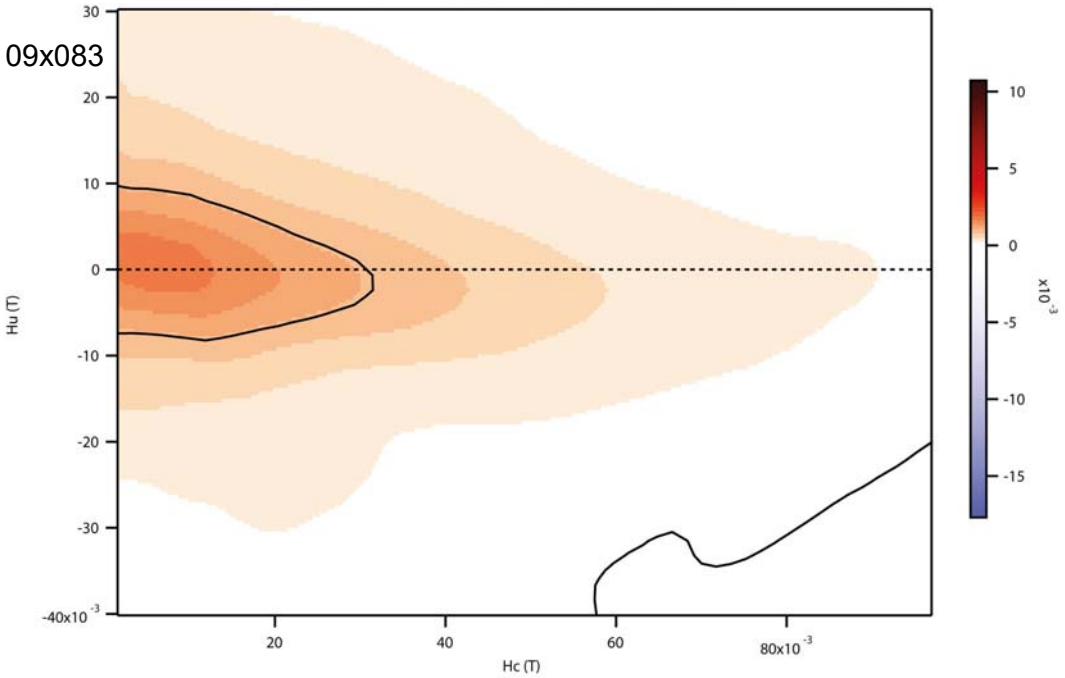
09x083
30
20
10
0
-10
-20
-30
-40x10 -3
Hu (T)
20
40
60
80x10 -3
Hc (T)
10
5
0
-5
-10
-15
x10-3

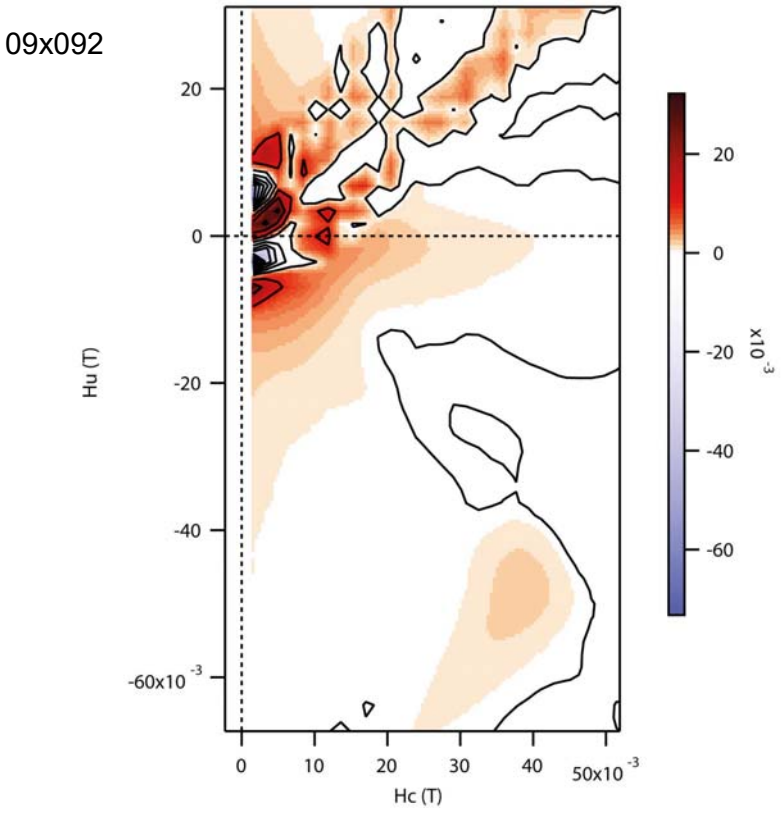
09x092
20
0
-20
-40
-60x10 -3
Hu (T)
0
10
20
30
40
50x10 -3
Hc (T)
20
0
-20
-40
-60
x10-3

42

43

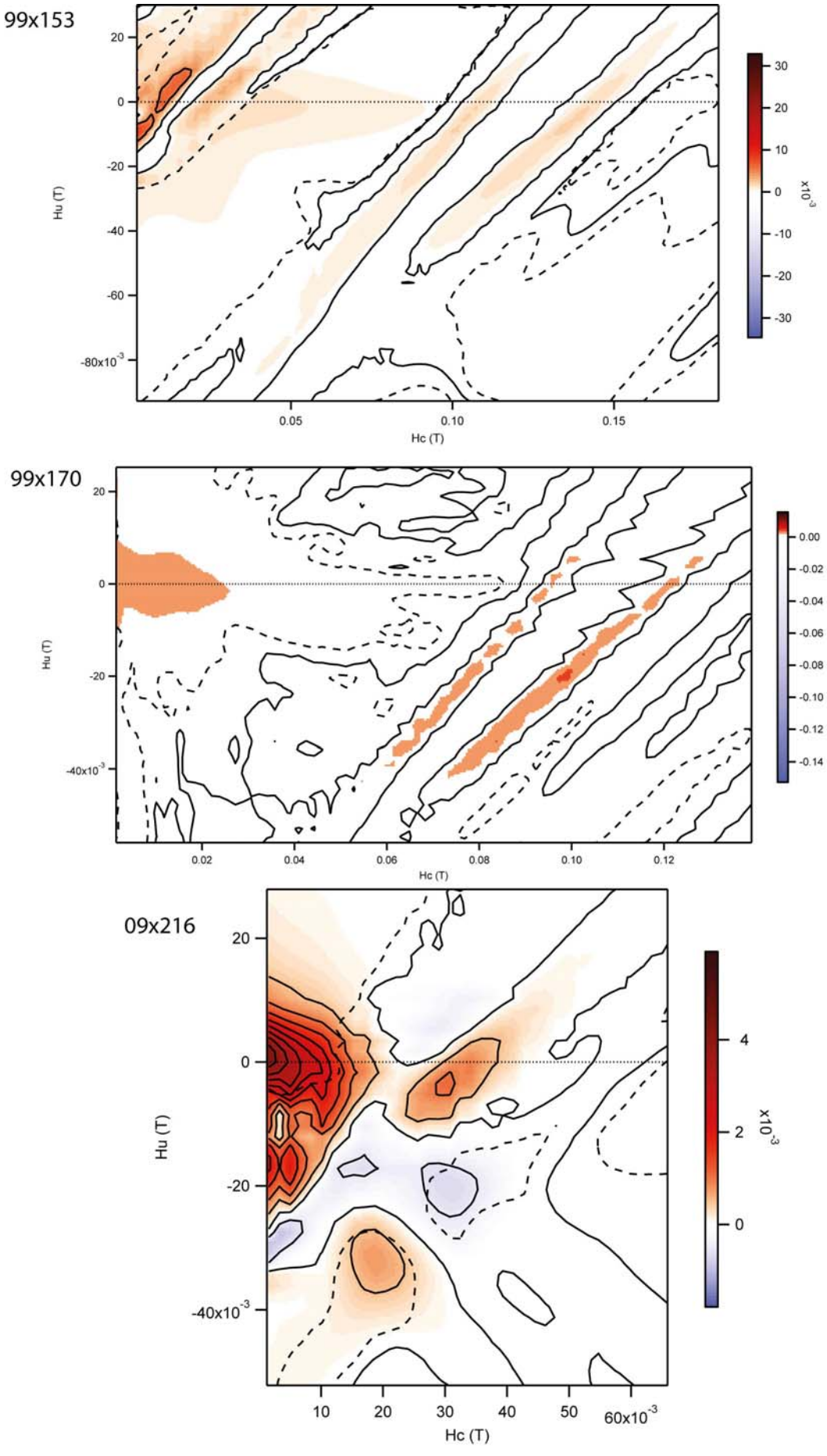
99x153
20
0
-20
-40
-60
-80x10-3
Hu (T)
0.05
0.10
0.15
Hc (T)
30
20
10
0
-10
-20
-30
x10-3
99x170
20
0
-20
-40x10-3
Hu (T)
0.02
0.04
0.06
0.08
0.10
0.12
Hc (T)
0.00
-0.02
-0.04
-0.06
-0.08
-0.10
-0.12
-0.14
09x216
20
0
-20
-40x10-3
Hu (T)
10
20
30
40
50
60x10-3
Hc (T)
4
2
0
x10-3

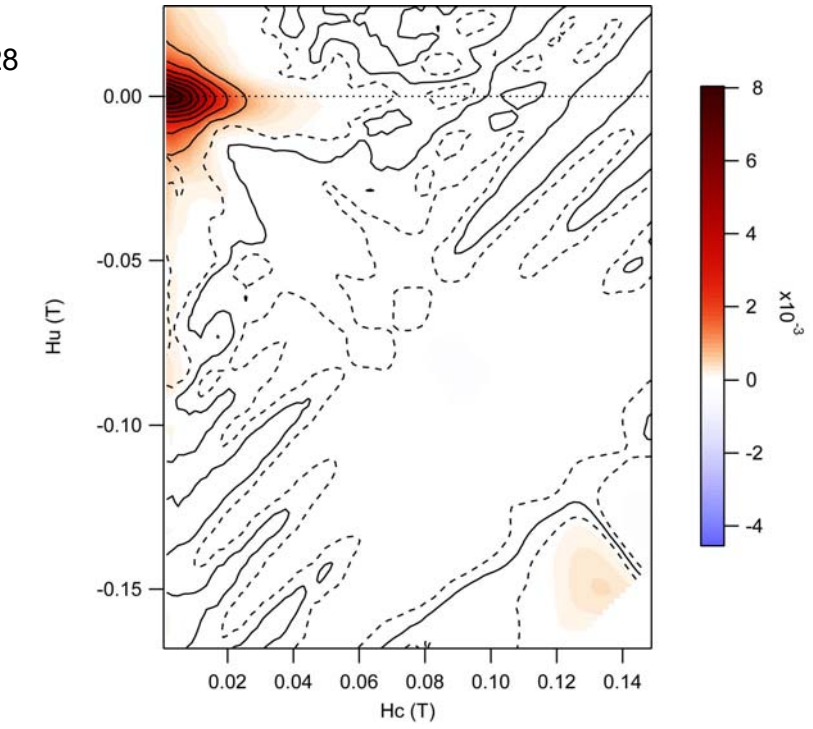

45

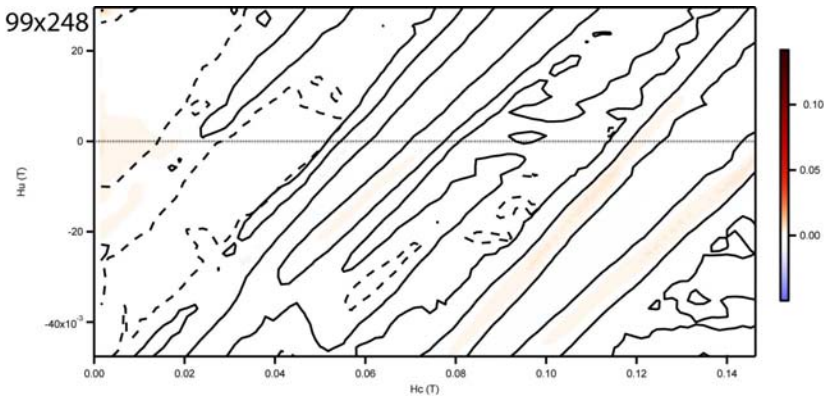

46

47 Figure DR5: FORC diagrams revealing the contribution of the SD, MD and PSD particles.

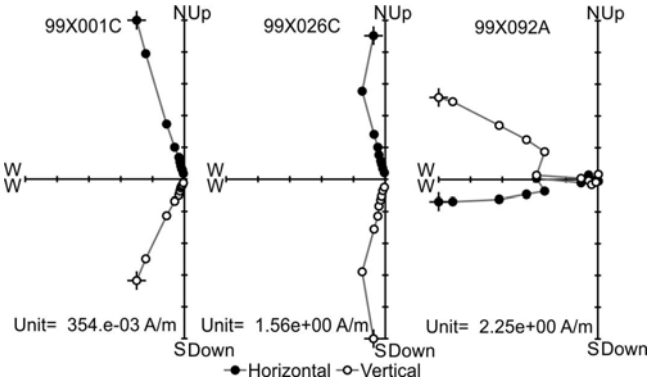

48

49 Figure DR6. Zijderveld demagnetization plots of three representative specimens with single,
50 double and multiple NRM components.

Table DR1: The measured bulk susceptibility (χ) and the Curie temperatures (Tc1, Tc2, and Tc3) are presented. Site 8 and 16 were not measured.

Site	χ (10^{-6} SI)	Tc1 (^{0}C)	Tc2 (^{0}C)	Tc3 (^{0}C)
1	48	132	-	531
3	43	100	439	558
4	215	-	433	-
5	56	-	-	522
6	58	-	-	518
7	72	203	-	521
9	65	202	-	513
10	229	221	-	-
11	140	267	489	-
12	33	224	424	595
13	74	335	-	518
14	90	251	474	-
17	93	238	460	527
21	73	-	-	544
22	76	70	-	556
23	156	154	457	-
24	35	-	-	522
25	74	-	437	-

Table DR2: Rotation (R) and flattening (F) experienced by the Xalapa Basalts, calculated by comparison with the GAPWaP (Torsvik et al., 2012). ΔR and ΔF calculated with the Demarest's method (Demarest, 1983).

Site	R	F	ΔR	ΔF
01	-24.6	3.9	16.9	8.5
03	-12.2	-4.9	10.3	6.7
04	31.7	19.6	8.1	3
05	2	7.9	7.9	4.1
06	-15.45	-0.9	5.4	3.75
07	0.8	-0.6	6.1	4
08	-44.8	5	27.2	12.6
09	-5.9	11.9	11.4	4.7
10	27.3	11.3	3.7	3.3
11	6	16.2	9.7	3
12	-17.7	12.8	7.2	3.4
13	5	16.4	15.7	5.1
14	-5.3	1.7	3.7	3
16	2.6	17.1	11.1	3.3
17	11.4	2.4	4.7	3.3
21	13	-19.9	12.3	3
22	-12.6	-6.3	4.8	3.2
23	-10.85	-0.7	5.2	3.6
24	26.6	-25.8	16.9	2.4
25	5.6	-13.2	3.6	3.3
26	-6.7	-12.4	13.2	5.5
27	-11.7	-3.1	16.2	8.7
37	123.2	-63.7	8.1	4.4

Table DR3: Rotation (R) and flattening (F) experienced by the El Castillo Ignimbrite, calculated by comparing ChRM directions provided by Alva-Valdivia et al. (2017) and the GAPWaP (Torsvik et al. 2012). ΔR and ΔF calculated with the Demarest's method (Demarest 1983).

Site	Paleo directions			R	F	ΔR	ΔF
	Dec	Inc	α95				
XA-02	156.9	-33.8	3.7	-21.5	-1.5	5.57	3.73
XA-15	158.8	-42.9	2	-19.6	7.6	2.85	2.78
XA-18	138.5	-18.1	3.5	-39.9	-17.2	9.21	3.61
XA-19	163.5	-36.5	2.8	-14.9	1.2	4.10	3.19
XA-20	160.1	-42	3	-18.3	6.7	3.93	3.31
XA-28	181.6	-4.3	8.1	3.2	-31.0	N.D.	6.87
XA-29	152.4	-47.3	10.5	-26.0	12.0	11.60	8.70
XA-30	350.7	37.2	9.1	-10.6	-3.9	12.24	7.63
XA-31	165.7	-30.9	4.4	-12.7	-4.4	7.06	4.19
XA-32	159.8	-23.9	2.6	-18.6	-11.4	5.39	3.08
XA-33	162.6	-46.6	5.7	-15.8	11.3	6.49	5.10
XA-34	156.3	-46.2	7.8	-22.1	10.9	8.82	6.64
XA-35	161.9	-43.8	5.9	-16.5	8.5	7.02	5.24
XA-38	169.3	-35.6	6.8	-9.1	0.3	9.53	5.90

References

Demarest, H.H., 1983. Error analysis for the determination of tectonic rotation from paleomagnetic data. J. Geophys. Res. Solid Earth 88, 4321–4328. doi:10.1029/JB088iB05p04321

Torsvik, T.H., Van der Voo, R., Preeden, U., Mac Niocaill, C., Steinberger, B., Doubrovine, P. V., van Hinsbergen, D.J.J., Domeier, M., Gaina, C., Tohver, E., Meert, J.G., McCausland, P.J.A., Cocks, L.R.M., 2012. Phanerozoic polar wander, palaeogeography and dynamics. Earth-Science Rev. 114, 325–368. doi:10.1016/j.earscirev.2012.06.007

Alva-Valdivia, L.M., Agarwal, A., Caballero-Miranda, C., García-Amador, B.I., Morales-Barrera, W., Rodríguez-Elizarraráz, S., Rodríguez-Trejo, A., 2017. Paleomagnetic and AMS studies of the El Castillo ignimbrite, central-east Mexico: Source and rock magnetic nature. J. Volcanol. Geotherm. Res. 336, 140–154. doi:10.1016/j.jvolgeores.2017.02.014